Article

Comparison Study on the Battery SoC Estimation with EKF and UKF Algorithms

Hongwen He *, Hongzhou Qin, Xiaokun Sun and Yuanpeng Shui

National Engineering Laboratory for Electric Vehicles, Beijing Institute of Technology, Beijing 100081, China; E-Mails: qhzbit@126.com (H.Q.); sxk_bit@163.com (X.S.); shuiyuanpeng@126.com (Y.S.)

* Author to whom correspondence should be addressed; E-Mail: hwhebit@bit.edu.cn;
Tel./Fax: +86-10-6891-4842.

Abstract: The battery state of charge (SoC), whose estimation is one of the basic functions of battery management system (BMS), is a vital input parameter in the energy management and power distribution control of electric vehicles (EVs). In this paper, two methods based on an extended Kalman filter (EKF) and unscented Kalman filter (UKF), respectively, are proposed to estimate the SoC of a lithium-ion battery used in EVs. The lithium-ion battery is modeled with the Thevenin model and the model parameters are identified based on experimental data and validated with the Beijing Driving Cycle. Then space equations used for SoC estimation are established. The SoC estimation results with EKF and UKF are compared in aspects of accuracy and convergence. It is concluded that the two algorithms both perform well, while the UKF algorithm is much better with a faster convergence ability and a higher accuracy.

Keywords: electric vehicles; dynamic modeling; SoC estimation; extended Kalman filter; unscented Kalman filter

1. Introduction

The battery, as an on-board electric energy storage source [1–3], is key to the development of electric vehicles (EVs). The state of charge (SoC) [4,5], which is the ratio of the battery's remaining available capacity to its rated capacity expressed as a percentage, is one of the key features in the battery management system [6,7]. However, in practical applications the SoC cannot be measured

directly, and its estimation becomes complicated due to the battery's complicated chemical reactions and uncertain influencing factors.

Techniques for battery SoC estimations can be categorized into three types [8–10]. The first type is the Coulomb counting method, which is an open-loop algorithm and could result in significant inaccuracies due to uncertain disturbances and difficulties to determine the initial value of SoC. The second type is look-up table method based on a black-box battery model, which describes the nonlinear relationship between SoC and its influencing factors. Although this approach can often produce a good estimation, it also causes problems like heavy computation burden and bad application in real-time. The third type is based on state estimation techniques with the state-space battery model, which is becoming more popular due to its advantages of being close-loop, online, and available to regulate the estimation error range dynamically.

The Extended Kalman Filter (EKF) [11–13] method is usually used in non-linear systems, using partial derivatives and first order Taylor series expansion to linearize the battery model. The Unscented Kalman filter [14–17] is a discrete-time filtering algorithm, which utilizes the unscented transform to solve filtering problems, and the UKF is able to accurately capture the posterior mean and covariance to the 3rd order of the Taylor series expansion. In this paper, for a lithium-ion battery, the EKF and UKF methods are both adopted in the SoC estimations based on the battery Thevenin model [18,19], and the estimation results are compared and discussed. The paper structure is arranged as follows: in Section 2, the battery is modeled and the model parameters are identified with experiments; In Section 3, the SoC estimation methods based on EKF and UKF, respectively, are proposed. In Section 4, simulation experiments are carried out and the results are presented and discussed in terms of accuracy and robustness. In Section 5, several concluding remarks are provided.

2. Battery Modeling

The equivalent circuit models that consist of resistances, capacitances and some other circuit components are selected to simulate the battery dynamic characteristics. At present, the Rint model, the Thevenin model, the RC model, and the PNGV model are generally applied to the simulation of batteries in EVs. The Thevenin model, as shown in Figure 1, is widely used to model the lithium-ion battery for its much better dynamic performance.

Figure 1. Schematic of the Thevenin model.
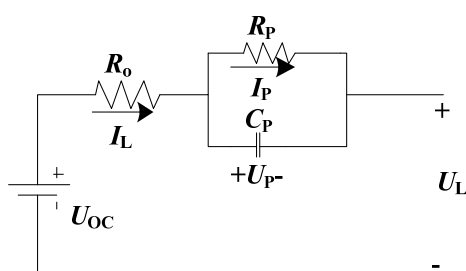
In Figure 1, there are three parts: the open circuit voltage U_{OC}, the internal resistances, and the equivalent capacitances. The internal resistances include ohmic resistance R_o and electrochemical polarization resistance R_p. The equivalent capacitance C_p simulates the battery electrochemical

polarization characteristics. The U_L is used to describe the terminal voltage, the U_p is used to describe the polarization voltage, the I_L is used to describe the load current and the I_P is used to describe the current across R_p. All the parameters in the model are related to SoC and temperature. Considering that all the experiments are conducted in a thermostat, the influence of temperature is ignored in this paper. The electrical behavior of the circuit model can be expressed as follows by Kirchhoff's current law (KCL) and Kirchhoff's voltage law (KVL):

$$\begin{cases} \dot{U}_P = \dfrac{I_L}{C_P} - \dfrac{U_P}{R_P C_P} \\ U_L = U_{OC} - U_P - I_L R_o \end{cases} \tag{1}$$
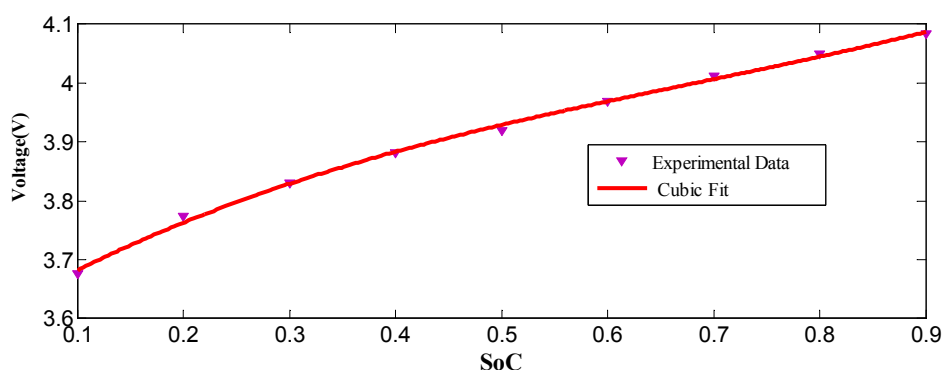
To acquire the parameters of the Thevenin model, the following charging and discharging experiments are carried out on a lithium-ion battery with nominal voltage of 3.6 V and nominal capacity of 31.5 Ah.

The Open-circuit voltage test: The test was performed to acquire the data to identify the parameters of the open-circuit voltage. The test procedure is as follows: the battery is fully charged at first and left in the open-circuit condition for 5 h until the change of the terminal voltage is negligible. Then the battery is discharged to 95% of the nominal capacity at a constant rate of 0.3 C, afterwards, it was left in the open-circuit condition again until the measured terminal voltage is considered to reach the equilibrium potential. The process was repeated at every 5% of the nominal capacity, all the open-circuit voltages at different SoCs are measured and a function of SoC is listed as Equation (2) by curve fitting.

$$U_{OC}(SoC) = 0.8921 \times SoC^3 - 1.5676 \times SoC^2 + 1.288 \times SoC + 3.5648 \tag{2}$$

The experimental data and the curve fitting result are shown in Figure 2.

Figure 2. The open-circuit voltage experimental data and curve fitting result.

The HPPC Test: The hybrid pulse power characterization (HPPC) test was performed to acquire the data to identify the parameters of ohmic resistance R_0. The test was conducted at 0.1 SoC intervals from 0.9 to 0.1, and the temperature was kept at 20 °C. Figure 3 shows one of the HPPC results at SoC = 0.9.
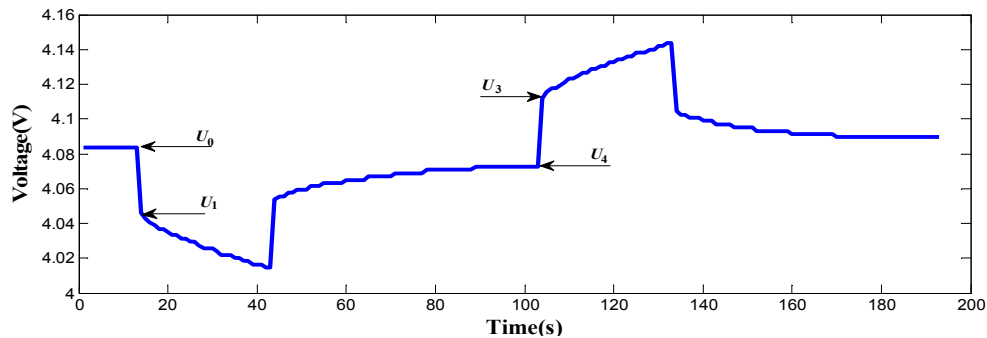
A voltage drop/rise appears when a pulse discharge/charge current I_L is loaded, then the ohmic resistance R_0 can be calculated by:

$$R_o = \frac{\Delta U}{|I_L|} \tag{3}$$

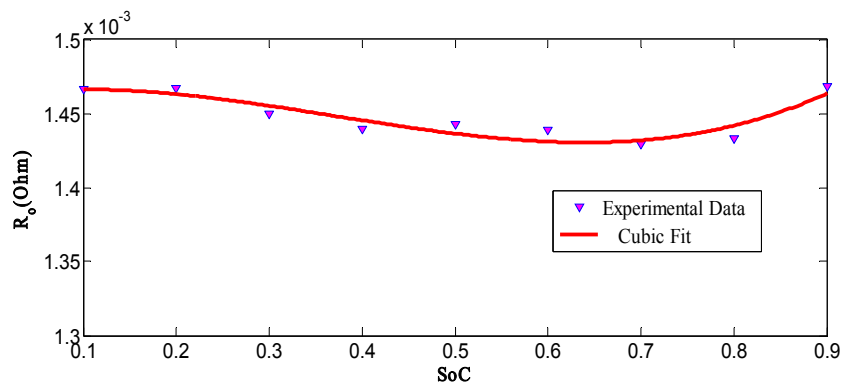The ΔU in Equation (3) is given by Equation (4) and marked in Figure 3:

$$\Delta U = \begin{cases} |U_1 - U_0| \\ |U_3 - U_2| \end{cases} \tag{4}$$

Figure 3. Battery voltage profile of one HPPC at SoC = 0.9.

Also, all the ohmic resistances at different SoCs are measured which is shown in Figure 4.

Figure 4. The Ohmic resistance experimental data and curve fitting result.

Finally, a function of SoC is listed as Equation (5) by curve fitting.

$$R_0(\text{SoC}) = -1.6693 \times 10^{-6}\,\text{SoC}^3 + 3.3387 \times 10^{-5}\,\text{SoC}^2 - 2.0059 \times 10^{-4}\,\text{SoC} + 0.0017911 \tag{5}$$

Based on the experiment data, the model parameters are identified as follows: we define a time constant $\tau = R_P C_P$, transform Equation (1) to a discrete system, then:

$$\begin{cases} U_{L,k} = U_{OC,k} - I_{P,k} R_{P,k} - I_{L,k} R_{o,k} \\ I_{P,k} = \exp(-\Delta t / \tau) \times I_{P,k-1} + (1 - \exp(-\Delta t / \tau)) \times I_{L,k-1} \end{cases} \tag{6}$$

where Δt denotes the sampling interval (1s in this paper); θ_k denotes the value of θ at time $k\Delta t$, here, θ refers to U_L, U_{OC}, I_P, R_P, R_o or I_L.

Multiple linear regression method was used in this paper; the linear regression accuracy can be evaluated by:

$$r^2 = \frac{\sum(\hat{U_L} - \overline{U_L})^2}{\sum(U_L - \overline{U_L})^2} \qquad (7)$$

where $\hat{U}_L$ is the observed value of U_L, and the $\overline{U_L}$ is the mean of U_L.

Based on the above method, some model parameters are listed in Table 1.

Table 1. The identified model parameters.

SoC	0.9	0.8	0.7	0.6
$R_0(\Omega)$	0.00147	0.00143	0.00143	0.00144
$R_P(\Omega)$	0.00331	0.00321	0.00312	0.00322
$C_P(F)$	3.0612×10^4	3.1469×10^4	3.1469×10^4	3.1250×10^4

The Beijing Driving Cycle (BJDC) [20] is chosen to validate the battery model and the corresponding load current profiles of ten BJDC cycles are shown in Figure 5. The terminal voltage results from test and model simulation were compared as shown in Figure 6. A statistic analysis on the voltage errors was performed, the results show that the maximum voltage error of the Thevenin model is 0.1402 V, the mean error is 0.0076 V, the variance is 1.8973×10^4 V^2 and the maximum error rate is 3.09%, which proves the reliability of this model.

Figure 5. The load current profile during ten BJDC cycles.
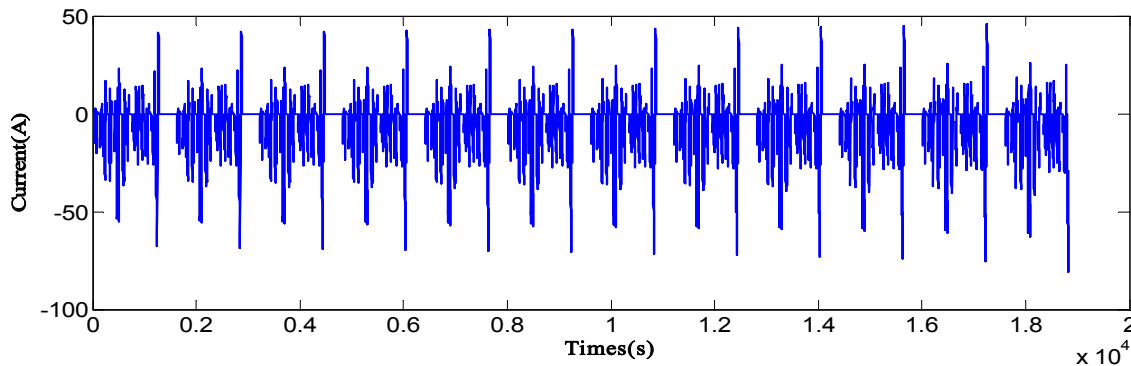
Figure 6. Comparisons between voltage of the model and the experiment.
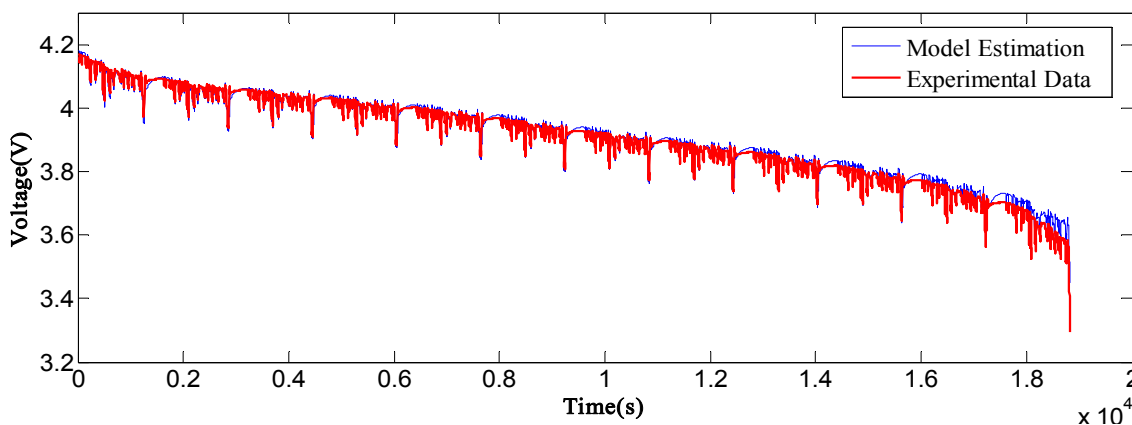
3. Battery SoC Estimations by EKF and UKF

The SoC is a relative quantity that describes the ratio of the remaining capacity to the present maximum available capacity of a battery [4,5], it is given by:

$$SoC_t = SoC_0 - \frac{1}{C_a}\int_0^t \eta I_{L,t}\mathrm{d}t \tag{8}$$

where SoC_t is the present SoC; SoC_0 is the initial value of SoC; C_a is the present maximum available capacity; η is the charge-discharge efficiency which is adopted as 100% herein.

Transform Equation (8) to a discrete form:

$$SoC_k = SoC_{k-1} - \frac{I_{L,k}\Delta t}{C_a} \tag{9}$$

3.1. Battery SoC Estimation with EKF

The EKF is a nonlinear version of Kalman filter after the nonlinear function is Taylor expanded and the quadratic term and high-order terms are ignored. A nonlinear discrete time system can be described as:

$$\begin{aligned}
x_k &= f_{k-1}(x_{k-1}, u_{k-1}, w_{k-1}) \\
y_k &= h_k(x_k, v_k) \\
&\begin{cases} w_k \sim (0, Q_k) \\ v_k \sim (0, R_k) \end{cases}
\end{aligned} \tag{10}$$

where x_k is the estimated state at time t_k; y_k is the output at time t_k; w_k is system excitation noise array; v_k is measure noise array; Q_k is variance matrix of the noise array of system; R_k is variance matrix of the measure noise array.

Transform Equation (1) to a discrete system:

$$\begin{cases} U_{L,k} = U_{OC,k} - U_{P,k} - I_L R_{o,k} \\ U_{p,k} = \exp(-\Delta t/\tau) \times U_{P,k\text{-}1} + \left(1 - \exp(-\Delta t/\tau)\right) \times I_{L,i\text{-}1} R_P \end{cases} \tag{11}$$

By combining Equation (1), Equation (9) and Equation (11), we select U_P, SoC as the state variables and U_L as the observable variable, then the standard state function is shown as Equation (12):

$$\begin{cases} \mathbf{x}_k = \mathbf{A}_{k-1}\mathbf{x}_{k-1} + \mathbf{B}_{k-1}\mathbf{u}_{k-1} + \mathbf{w}_{k-1} \\ \mathbf{y}_k = \mathbf{C}_k\mathbf{x}_k + \mathbf{D}_k\mathbf{u}_k + \mathbf{v}_k \end{cases} \tag{12}$$

where $\mathbf{x}_k = \begin{pmatrix} U_{P,k} \\ SoC_k \end{pmatrix}$; $\mathbf{y}_k = [U_{L,k}]$; $\mathbf{A}_k = \begin{pmatrix} \exp(-\Delta t/\tau) & 0 \\ 0 & 1 \end{pmatrix}$; $\mathbf{B}_k = \begin{pmatrix} R_P(1\text{-}\exp(-\Delta t/\tau)) \\ \Delta t/C_a \end{pmatrix}$;

$\mathbf{C}_k = [-1 \quad \frac{\mathrm{d}U_{oc}}{\mathrm{d}SoC} - I_{L,k} \times \frac{\mathrm{d}R_0}{\mathrm{d}SoC}]$; $\mathbf{D}_k = [-R_0]$. The calculation based on EKF can be summarized as Figure 7.

Figure 7. The SoC estimation flow based on EKF.
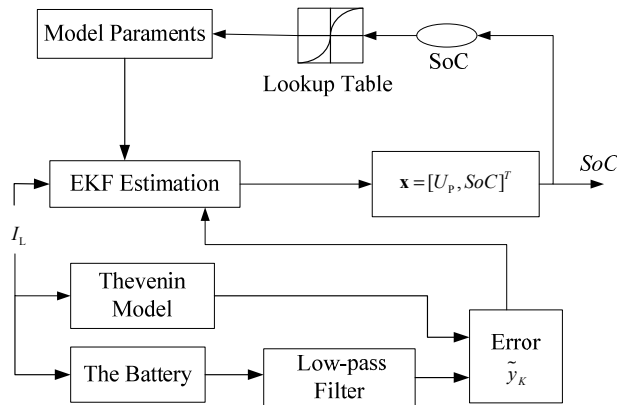
3.2. Battery SoC Estimation with UKF

Considering that high orders are ignored in EKF, UKF is proposed to solve the filtering problem in some severe nonlinear systems. Based on the idea that it is easier to approximate the probability density of the nonlinear function than the nonlinear function itself, the unscented Transform (UT) [13,14] is applied in UKF, which can be described as follows:

Assuming **x** has mean $\bar{x}$ and covariance P_x, a set of 2n + 1 (n ,the state dimension) sigma points can be chosen [21], which is shown in Equation (13):

$$\begin{cases} x_0 = \bar{x} \\ x_i = \bar{x} + (\sqrt{(n+\lambda)P_x})_i, i = 1,2.......n, \\ x_i = \bar{x} - (\sqrt{(n+\lambda)P_x})_i, i = n+1,.......2n \end{cases} \tag{13}$$

The set of points can approximate the Gaussian distribution of the state **x**.

Non-linear transform all the points: All the points would be non-linear transformed in this step according to non-linear function. The results can be expressed as:

$$Y_i = f(x_i) \tag{14}$$

The distribution of **y** = *f*(**x**) can be approximately revealed by the set of sigma points {y_i}.

Calculate the mean value and covariance: The mean value and covariance of *y* can be obtained after being weighted:

$$\begin{cases} \bar{y} \approx \sum_{i=0}^{2n} W_i^{(m)} Y_i \\ P_y \approx \sum_{i=0}^{2n} W_i^{(c)} (Y_i - \bar{y})(Y_i - \bar{y})^T \\ W_0^{(m)} = \kappa / (n+\kappa) \\ W_0^{(c)} = \kappa / (n+\kappa) + (1 - \alpha^2 + \beta) \\ W_i^{(m)} = W_i^{(c)} = \kappa / [2(n+\kappa)], i = 1,2,...,2n \end{cases} \tag{15}$$

where $W_i^{(m)}$ and $W_i^{(c)}$ are separately the weight factors of the mean value and the covariance. The above process can be described as Figure 8:

Figure 8. UT Transform.
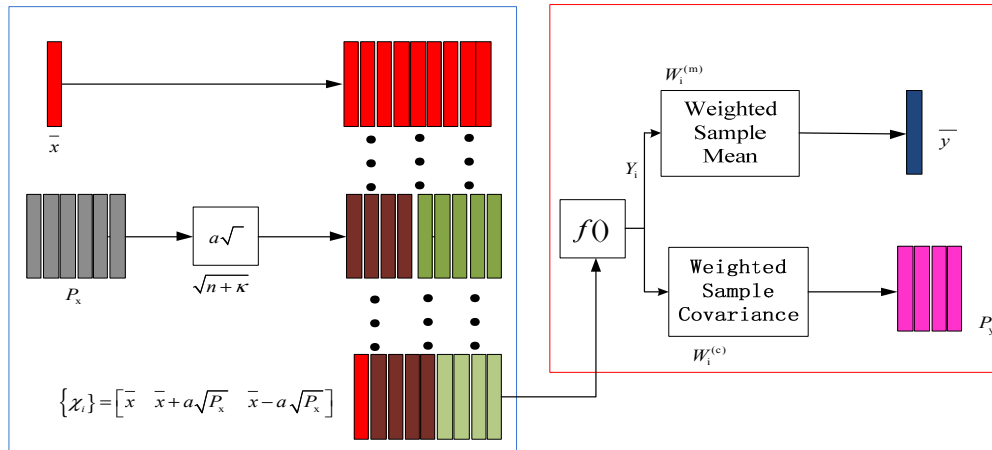
Estimate using standard kalman filter: For SoC estimation, the state space is the same as EKF, so we simply illustrate the unscented Kalman filter algorithm as follows:

Initialization:

$$\overline{x_0} = E(x_0), \quad P_0 = E[(x_0 - \overline{x_0})(x_0 - \overline{x_0})^T]$$ (16)

State estimation:

(a) Generate sigma points and their weight factors at time step $k - 1$

$$\begin{cases} x_0 = \overline{x} \\ x_i = \overline{x} + (\sqrt{(n + \lambda)P_x})_i, i = 1, 2.......n \\ x_i = \overline{x} - (\sqrt{(n + \lambda)P_x})_i, i = n + 1,.......2n \end{cases}$$ (17)

(b) Time is updated:

State estimate time update:

$$x_{k|k-1} = f\left(x_{k-1}, x_{k-1}^v\right), \overline{x}_{k|k-1} = \sum_{i=0}^{2n} W_i^{(m)} x_{i,k|k-1}$$ (18)

Error covariance time update:

$$P_{x,k|k-1} = \sum_{i=0}^{2n} W_i^{(c)} \left[x_{i,k|k-1} - \overline{x}_{k|k-1}\right]\left[x_{i,k|k-1} - \overline{x}_{k|k-1}\right]^T$$ (19)

Output estimate time update:

$$Y_{k|k-1} = g\left(x_{k|k-1}, x_{k-1}^n\right), \overline{y}_{k|k-1} = \sum_{i=0}^{2n_a} W_i^{(m)} Y_{i,k|k-1}$$ (20)

(c) Measurement is updated:

Estimator gain matrix:

$$\begin{cases} P_{y,k} = \sum_{i=0}^{2n} w_i^c (Y_{i,k|k-1} - \overline{y})(Y_{i,k|k-1} - \overline{y})^T \\ P_{xy,k} = \sum_{i=0}^{2n} w_i^c (Y_{i,k|k-1} - \overline{x})(Y_{i,k|k-1} - \overline{y})^T, L = P_{xy,k} * P_{y,k}^{-1} \end{cases} \quad (21)$$
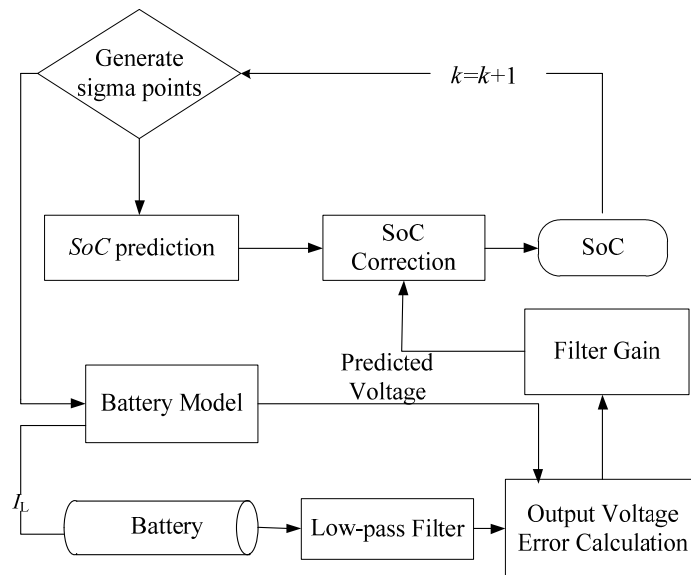
State estimate update:

$$\hat{\mathbf{x}}_k = \hat{\mathbf{x}}_k^- + \mathbf{L}(\mathbf{y}_k - \hat{\mathbf{y}}_k^-) \quad (22)$$

Error covariance measurement update:

$$\mathbf{P}_{x,k} = \mathbf{P}_{x,k}^- - \mathbf{L}\mathbf{P}_{y,k}\mathbf{L}^T \quad (23)$$

The process can be expressed as shown in Figure 9:

Figure 9. SoC estimation based on UKF.

4. Experiments and Discussion

BJDC is selected to evaluate the EKF algorithm and the UKF algorithm in SoC estimation. In this paper, ten periods of BJDC are employed to verify the SoC estimation approach. The current profiles sampled during consecutive BJDC cycles are shown in Figure 5.

For EKF and UKF, the initial parameters are specified the same as follows:

$$\begin{aligned} A &= \begin{bmatrix} 0.9910 & 0 \\ 0 & 1 \end{bmatrix} \\ B &= \begin{bmatrix} 2.8800\text{e-}005 & 8.9606\text{e-}006 \end{bmatrix}^T \\ C &= \begin{bmatrix} 1 & 3.8809 \end{bmatrix}^T \\ D &= \begin{bmatrix} 0.0014 \end{bmatrix} \end{aligned} \quad (24)$$

Figure 10 describes the terminal voltage curves. The error of the two algorithms are showed in Figure 11, from which it could be easily concluded that the UKF algorithm can modulate the error

more effectively and estimate the terminal voltage more precisely. A detailed comparison of the terminal voltage between EKF and UKF is presented in Table 2.

Figure 10. Voltage profiles of 10 consecutive BJDC cycles.
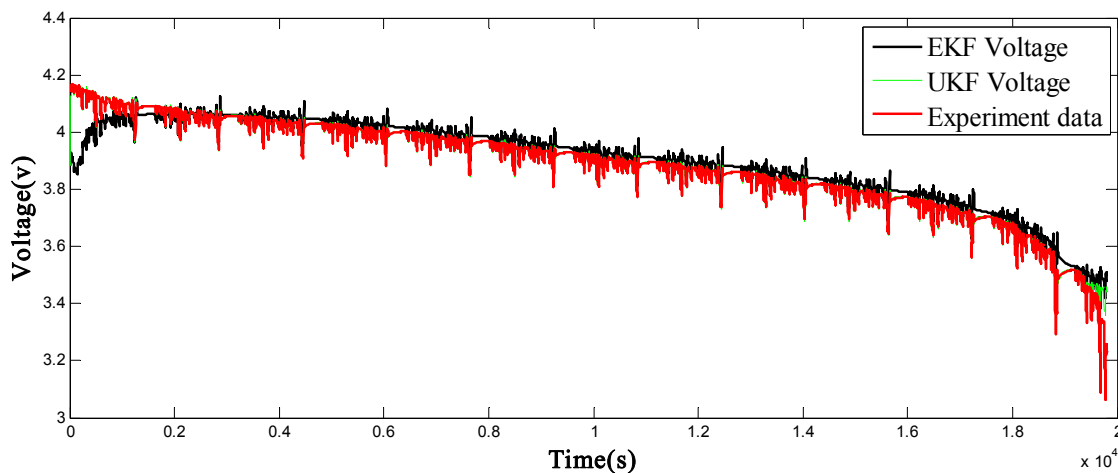
**Figure 11.** Terminal voltages and voltage error comparisons between UKF and EKF.
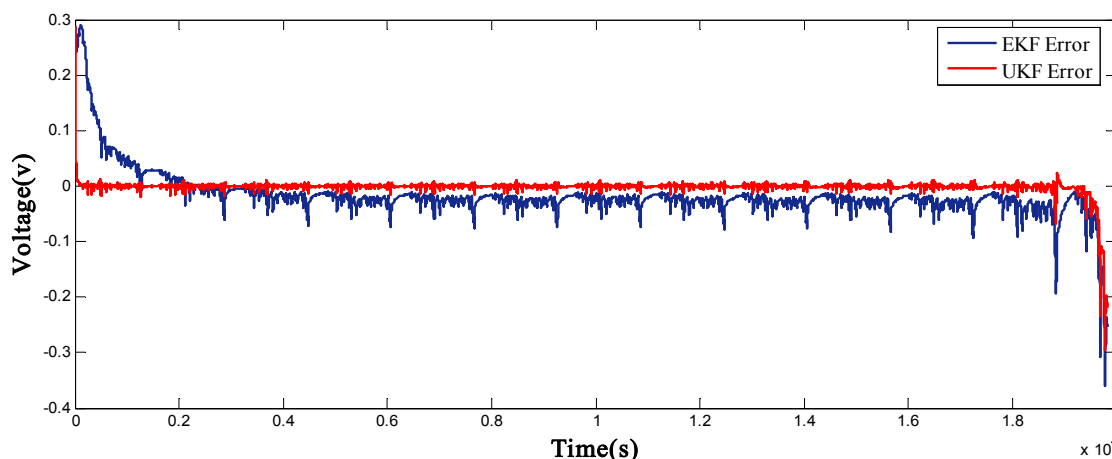
**Table 2.** The Statistic list of Voltage Errors for EKF and UKF.

Index	Max	Mean	Variance
EKF	0.3595	0.0064	3.0196×10^{-4}
UKF	0.2950	0.0038	5.4716×10^{-4}

To validate the availability of EKF and UKF, different initial SoCs are set. Figure 12 shows the performance of EKF while the results of UKF are shown in Figure 13. It is obvious that both algorithms can solve the initial estimation inaccuracy of SoC and track the experimental data changes. Also, it could be concluded that the convergence rate would be reduced with the increase of initial error, but the UKF algorithm could still converge to the real value rapidly while EKF has lost the ability when the initial SoC was set at 0.1. Moreover, compared with UKF, EKF has a larger overshoot.

**Figure 12.** SoC estimation curves with different initial SoCs with EKF.
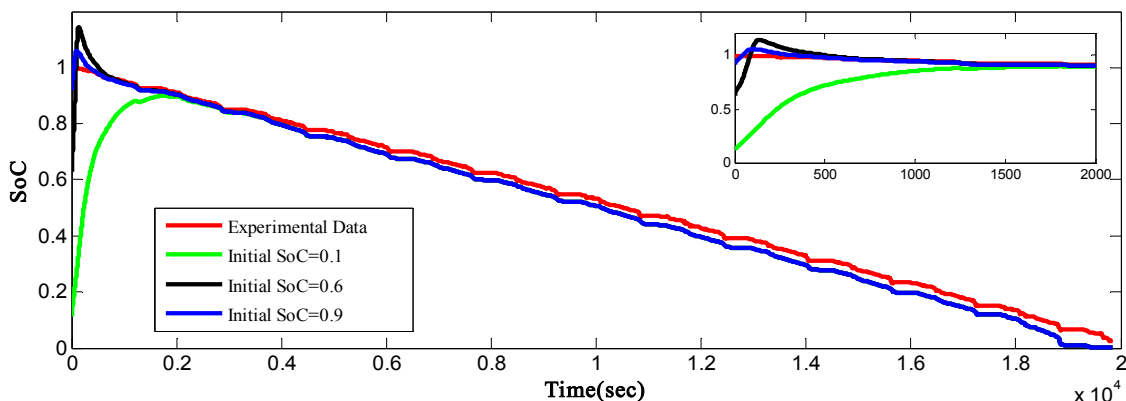
Figure 13. SoC estimation curves with different initial SoCs with UKF.
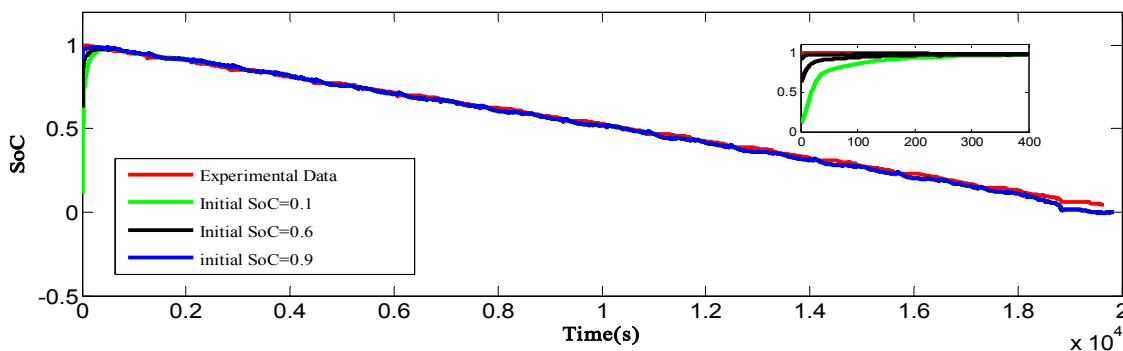
From Figure 14, it can be easily seen that UKF has a better performance in tracking the change of SoC and a faster convergence speed compared with EKF. Detailed comparisons are carried out and the results listed in Table 3. The maximum error between EKF and UKF is equal as the initial SoC is exactly the same. For UKF, the absolute mean error is only 1.66% and the error variance is 0.00095, while the corresponding values in EKF are 4.42% and 0.0072 respectively. In theory, the EKF's ignoring the second-order and higher-order entries will greatly affect the estimate accuracy. Moreover, the computational effort of UKF is reduced to a great extent as it is not required to calculate the Jacobian matrixs. As a result, the UKF can overcome the traditional EKF method's shortcomings such as slow convergence speed and low precision.

Figure 14. SoC estimation curves with 0.1 of initial SoC.
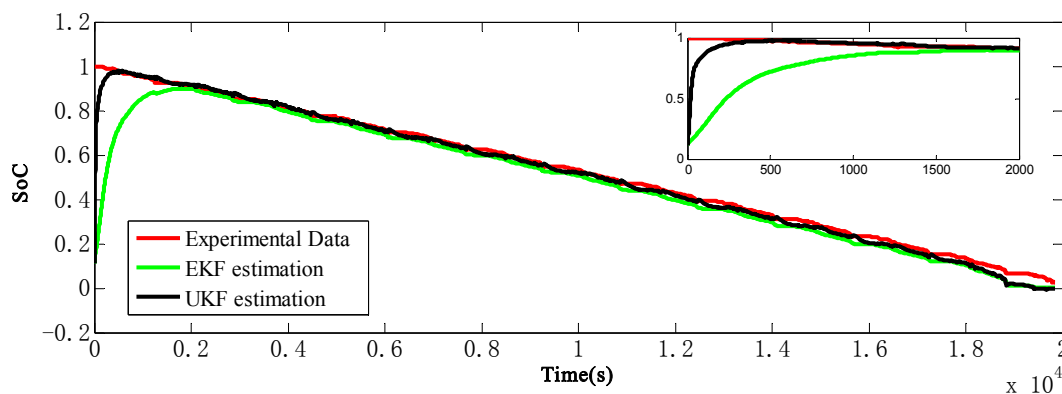
Table 3. Comparison of SoC error.

Index	Max	Mean	Variance
UKF	90.00%	1.66%	0.00095
EKF	90.00%	4.42%	0.0072

Besides, the results also show that there is a noticeable error increase especially when the battery SoC is very low(under 5%), this is mainly caused by the high nonlinear operating performance of the battery when it is near empty and the Thevenin model needs to be improved at that time.

5. Conclusions

The Thevenin model is adopted, and its parameter identification is performed based on related experimental data. The experiment and simulation results show that the maximum error of the model is within 3.09%, and the mean error is 0.0076 V. The model has the ability to support the EKF-based and UKF-based SoC estimation. Both the EKF algorithm and UKF algorithm could solve the initial estimation inaccuracy of SoC and track the change of SoC effectively, but UKF performs better with a mean error of 1.66% and a faster convergence speed which is related to the initial SoC values. One point that should be figured out is that the performance of the battery is connected with the temperature. Due to the condition limits, the effect of temperature is not taken into consideration in this paper. Future work would center on the effect of temperature and the realization of the algorithm on hardware.

Conflicts of Interest

The authors declare no conflict of interest.

References

1. *One Million Electric Vehicles by 2015: February 2011 Status Report*; US Department of Energy: Washington, DC, USA, 2011.
2. He, H.; Yan, S.; Xiao, Z. Integrated control method for a fuel cell hybrid system. *Asia-Pac. J. Chem. Eng.* **2009**, *1*, 68–72.
3. Kennedy, B.; Patterson, D.; Camilleri, S. Use of lithium-ion batteries in electric vehicles. *J. Power Sources* **2000**, *2*, 156–162.
4. Åhman, M. Primary energy efficiency of alternative powertrains in vehicles. *Energy* **2001**, *26*, 973–989.
5. Chaturvedi, N.L.; Klein, R.; Christensen, J.; Ahmed, J.; Kojic, A. Algorithms for advanced battery-management systems. *IEEE Control Syst. Mag.* **2010**, *3*, 49–68.

6. Piller, S.; Perrin, M.; Jossen, A. Methods for state-of-charge determination and their applications. *J. Power Sources* **2001**, *96*, 113–120.

7. Aylor, J.H.; Johnson, B.W. A battery state-of-charge indicator for electric wheelchairs. *IEEE Trans. Ind. Electron.* **1992**, *39*, 398–409.

8. Liu, T.; Chen, D.; Fang, C. Design and implementation of a battery charger with a state-of-charge estimator. *Int. J. Electron.* **2000**, *87*, 211–226.

9. He, H.; Xiong, R.; Zhang, X.; Sun, F.; Fan, J. State-of-charge estimation of the lithium-ion battery using an adaptive extended Kalman filter based on an improved Thevenin model. *IEEE Trans. Veh. Technol.* **2011**, *60*, 1461–1469.

10. Plett, G.L. Extended Kalman filtering for battery management systems of LiPB-based HEV battery packs—Part 3. State and parameter estimation. *J. Power Sources* **2004**, *2*, 277–292.

11. Han, J.; Kim, D.; Sunwoo, M. State-of-charge estimation of lead-acid batteries using an adaptive extended Kalman filter. *J. Power Sources* **2009**, *2*, 606–612.

12. Vasebi, A.; Partovibakhsh, M.; Bathaee, S. A novel combined battery model for state-of-charge estimation in lead-acid batteries based on extended Kalman filter for hybrid electric vehicle applications. *J. Power Sources* **2007**, *1*, 30–40.

13. Shi, P.; Zhao, Y. Application of Unscented Kalman Filter in the SoC Estimation of Li-Ion Battery for Autonomous Mobile Robot. In Proceedings of the IEEE International Conference on Information Acquisition, Weihai, China, 20–23 August 2006; pp. 1279–1283.

14. He, H.; Xiong, R.; Fan, J. Evaluation of lithium-ion battery equivalent circuit models for state of charge estimation by an experimental approach. *Energies* **2011**, *4*, 582–598.

15. Xiong, K.; Chan, C.; Zhang, H. Detection of satellite attitude sensor faults using the UKF. *IEEE Trans. Aerosp. Electron. Syst.* **2007**, *2*, 480–491.

16. Mirzaee, A.; Salahshoor, K. Fault diagnosis and accommodation of nonlinear systems based on multiple-model adaptive unscented Kalman filter and switched MPC and H-infinity loop-shaping controller. *J. Process Control.* **2012**, *3*, 626–634.

17. He, H.; Xiong, R.; Guo, H. Online estimation of model parameters and state-of-charge of LiFePO$_4$ batteries in electric vehicles. *Appl. Energy* **2012**, *89*, 413–420.

18. Roscher, M.; Sauer, D. Dynamic electric behavior and open-circuit-voltage modeling of LiFePO$_4$-based lithium ion secondary batteries. *J. Power Sources* **2011**, *196*, 331–336.

19. He, H.; Zhang, X.; Xiong, R.; Xu, Y.; Guo, H. Online model-based estimation of state-of-charge and open-circuit voltage of lithium-ion batteries in electric vehicles. *Energy* **2012**, *39*, 310–318.

20. Xiong, R.; He, H.; Sun, F.; Zhao, K. Online estimation of peak power capability of Li-ion batteries in electric vehicles by hardware-in-loop approach. *Energies* **2012**, *5*, 1455–1469.

21. Rudolf, M. Sigma-Point Kalman Filters for Probabilistic Inference in Dynamic State-Space Models. Ph.D. Thesis, OGI School of Science & Engineering at Oregon Health & Science University, Portland, OR, USA, April 2004.